https://doi.org/10.22226/2410-3535-2022-2-148-152

Graphene nanoflakes and fullerenes doped with aluminum: features of Al-C interaction and adsorption characteristics of carbon shell

K. P. Katin[†,1,2], S. Kaya[3], M. M. Maslov[1,2]

[†]KPKatin@yandex.ru

[1]Laboratory of Computational Design of Nanostructures, Nanodevices, and Nanotechnologies, Research Institute for the Development of Scientific and Educational Potential of Youth, Moscow, 119620, Russia
[2]Institute of Nanotechnologies in Electronics, Spintronics and Photonics, National Research Nuclear University "MEPhI", Moscow, 115409, Russia
[3]Department of Chemistry, Faculty of Science, Cumhuriyet University, Sivas, 58140, Turkey

The aluminium-carbon interaction in two core-shell systems (Al_{22} nanoparticle coated with graphene nanoflake and $Al@C_{60}$ metallofullerene) is investigated within the density functional theory. A set of non-equilibrium configurations of the coated Al_{22} nanoparticle is obtained from the *ab initio* molecular dynamics simulation. The Morse parameters describing the Al-C interaction are fitted based on density functional calculations performed at the B3LYP/6-31G* level of theory. The Grimme's D3 dispersion corrections are added to accurately account for the non-covalent interactions. It is shown that the concave carbon surface interacts much weaker with the nanoparticle and is located further away from it compared to the usually considered convex surfaces. Negligible charge transfer from aluminum core to carbon shell confirms that Al_{22} nanoparticle do not change the shell reactivity. In contrast, a single Al atom endohedrally doped C_{60} fullerene strongly interacts with the carbon cage and distorts the frontier molecular orbitals and reactivity of the compound. We also compare the hydrogen F..H-O bonds formed between the fluorinated $C_{60}F_2$ or $Al@C_{60}F_2$ cages and niacin drug molecule. We found that Al leads to drastic weakening of this hydrogen bond. We conclude that Al_{22} nanoparticle do not change reactivity of the carbon shell, whereas a single Al atom reduces reactivity of the outer fullerene.

Keywords: aluminum nanoparticle, crumped graphene, Morse potential, drug delivery, metallofullerenes.

1. Introduction

Composite materials based on the carbon structures doped with metal nanoparticles are widely used in many fields [1]. The high adsorption capacity of the carbon surface to most metals ensures their reliable loading. In addition, metal nanoparticles on the carbon surface possess uniform distribution without aggregation and demonstrate improved adsorption and catalytic activity [2]. Therefore, such composite structures are used for drug delivery [3–4], hydrogen storage [5–6], catalytic splitting of water [7–8] and in other fields [9–10]. In recent years, researchers developed many techniques for synthesizing metal-carbon nanocomposites. Electrochemical deposition, microwave irradiation, microfluidic-based strategies as well as thermal, chemical or photochemical reduction are commonly used (see Refs. [11–12] and references therein).

Here, we focus on aluminum as a promising dopant for carbon nanostructures. Aluminum is the most common metal in the Earth's crust. Its lightness, corrosion resistance and other physicochemical properties make aluminum an attractive material for many fields. For example, carbon structures doped with aluminum are used as adsorbents [13–14], hydrogen storage systems [15–16], catalysts [17] and drugs carriers [18]. The interest to aluminum for medical applications is associated with some additional advantages of this metal. Monteiro-Riviere et. al. shown that aluminum nanoparticles do not reduce viability of human neonatal epidermal keratinocytes [19]. Watterson et. al. reported that the addition of the Al layer increased the mechanical integrity of the interface retinal implant devices based on carbon nanotubes and enhanced retinal neurite outgrowth [20]. Recently, Zhao et. al. fabricated and characterized a highly effective dual-stimuli responsive porous aluminum nano membrane which provide controllable and sustainable drug release [21].

The most common way to use aluminum for the drug delivery is based on the ability of the Al atom to be embedded in the carbon surface by replacing the carbon atom. As a result, Al atom forms a site with increased reactivity on the surface of a fullerene [22], nanotube [23] or graphene [24]. Then drugs can be easily adsorbed on the embedded Al atom. A less studied method implies using of nanoparticles with an aluminum core wrapped in a ligand shell [25–26]. In such delivery systems, aluminum does not interact with the drug directly, but affects the physicochemical properties of the shell.

In this Letter, we present a quantum chemical study of aluminum nanoparticles wrapped in carbon shells. The nanostructures $Al_{22}@C_{250}H_{52}$ and metallofullerene $Al@C_{60}$ are considered as models of the drugs delivery systems. Consideration of two models of different sizes provides an understanding of the influence of the system size on its properties. We studied the intensity of the Al-C interaction and the effect of aluminum on the adsorption properties of a carbon shell.

2. Computational Details

The atomistic model of the considered $Al_{22}@C_{250}H_{52}$ system is shown in Fig. 1. It includes the Al_{22} nanoparticle (Fig. 1a) coated by the graphene (Fig. 1b). Diameters of the Al nanoparticle and carbon shell are about 0.6 and 1.5 nm, respectively. Similar flakes were previously used to model crumpled graphene [27–29]. However, they can also represent concave sections of compressed graphene sheet as well as the inner surfaces of pores, nanotubes, and fullerenes. The nanoflake's edges were passivated with the hydrogen atoms to avoid dangling bonds with increased activity. The metallofullerene $Al@C_{60}$ consists of a single Al atom placed inside the common C_{60} cage with the I_h symmetry (Fig. 1c).

Ab initio molecular dynamics and optimization was performed within the density functional theory with a hybrid exchange-correlation B3LYP functional [30–31] and an electronic basis set 6-31G* [32]. Empirical corrections of D3 [33] were taken into account for an accurate description of non-covalent interactions. The high-performance TeraChem software [34] developed for GPU-accelerated molecular dynamics ensured the simulations running in an acceptable time. Geometry relaxation of all systems were performed until energy change, maximal energy gradient and root-mean-square gradient become lower than 10^{-6} Hartree, $4.5 \cdot 10^{-4}$ Hartree/Bohr and $3.0 \cdot 10^{-4}$ Hartree/Bohr, respectively. These are the default thresholds implemented in TeraChem.

The interaction energy E between the nanoparticle and the graphene flake was calculated by the formula

$$E_{DFT} = E(Al_{22}) + E(\text{nanoflake}) - E(Al_{22} + \text{nanoflake}). \quad (1)$$

Here $E(Al_{22} + \text{nanoflake})$, $E(Al_{22})$ and $E(\text{nanoflake})$ correspond to the total energies of the entire system, aluminum nanoparticle and nanoflake, respectively. The encapsulation energy E_{inc} of an aluminum atom into a fullerene was calculated similarly

$$E_{enc} = E(Al) + E(C_{60}) - E(Al@C_{60}). \quad (2)$$

To probe the adsorption properties of the considered drugs delivery systems, we adsorbed the niacin molecule on them. Niacin is a form of vitamin B_3, which is widely used in pharmacology. We selected niacin for the adsorption test, because this small molecule contains a carboxyl group (see Fig. 1d), which can form the hydrogen bonds with carriers. Such type of bonding is typical for the most drugs adsorbed on the carbon fullerenes functionalized with fluorine, oxygen or other electronegative elements. To calculate the binding energy E_b between the carrier and the drug, we used a similar formula.

$$E_b = E(\text{carrier}) + E(\text{niacin}) - E(\text{carrier} + \text{niacin}). \quad (3)$$

Note that with such a definition, high positive values of E_{DFT}, E_{enc} and E_b correspond to a strong attraction between the components of the considered complexes.

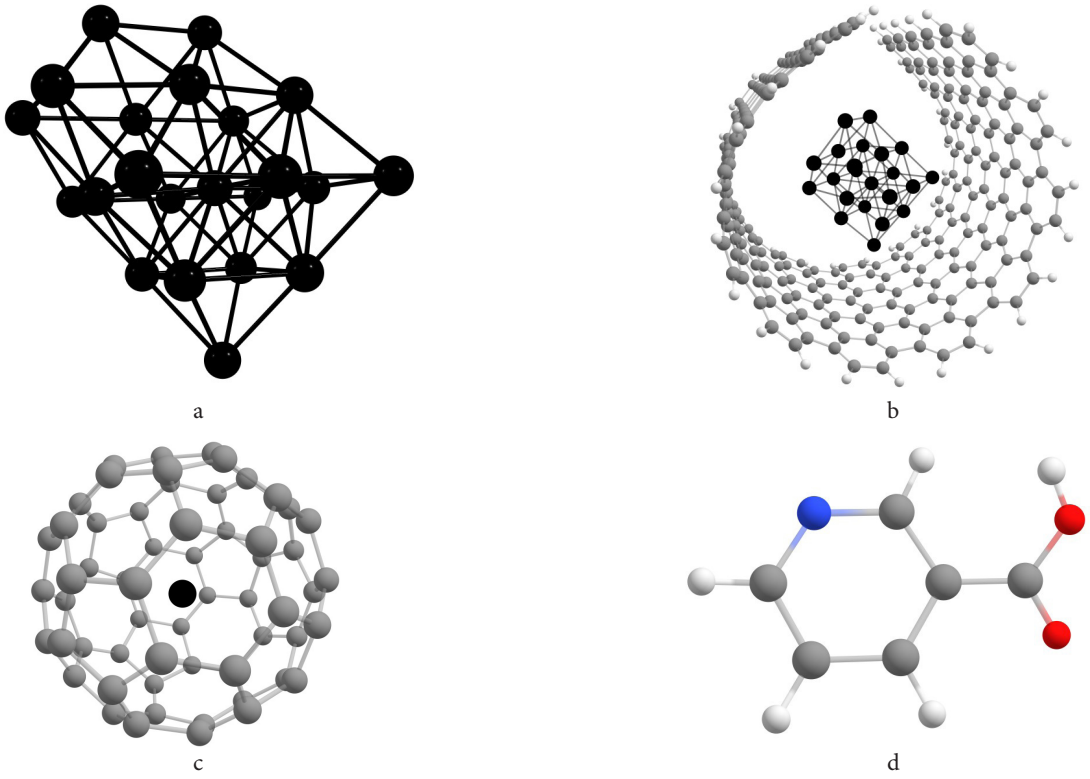

Fig. 1. (Color online) The atomistic model of the considered systems: Al_{22} nanoparticle (a) coated by the carbon nanoflake $C_{250}H_{52}$ (b), $Al@C_{60}$ metallofullerene (c) and niacin drug (d). Black, gray, blue, red and white balls represent aluminum, carbon, nitrogen, oxygen and hydrogen atoms.

3. Results and Discussion

3.1. Weak interaction between Al_{22} nanoparticle and $C_{250}H_{52}$ nanoflake

First, we optimized the geometry of the $Al_{22}@C_{250}H_{52}$ system shown in Fig. 1b. After optimization, the minimum Al-C distance exceeded 3 Å, indicating weak interaction. Note that Qiu et al. reported the much shorter equilibrium Al-C distance of 2.246 Å [35]. We are not surprised by this discrepancy, because Qiu considered the convex surface of the nanotube, whereas we consider the concave one. As is known, the concave surface has a much lower chemical activity and, therefore, is located farther from the nanoparticle (see Ref. [36] and references therein). Moreover, total Mulliken charge of Al_{22} nanoparticle is lower than 0.01*e*, indicating the absence of charge transfer from the carbon to aluminum atoms. Therefore, we conclude that aluminum nanoparticle does not affect the reactivity of carbon nanoflake.

3.2. Morse parameters for interaction between Al_{22} nanoparticle and $C_{250}H_{52}$ nanoflake

To deeper investigate the interaction in the $Al_{22}@C_{250}H_{52}$ system, we derived the Morse parameters for Al-C interaction. In contrast to complicated density functional approach, Morse parameters provides a simple and physically clear estimation of interaction energy, optimal interatomic distance and bond rigidity. In addition, *ab initio* methods are often supplemented with empirical approaches that provide helpful insight into the system behavior on a larger scale [37]. Sometimes researchers prefer to use simplified approaches such as pair Morse potentials for carbon-metal interaction because more sophisticated empirical potentials do not provide higher accuracy [38 – 40]. Lyalin and co-workers noted that "Morse potential allows us to study the influence of the parameters on the thermodynamic properties, keeping a clear physical picture of the process occurring in the system" [41]. Morse parameters for metal-carbon interaction were proposed and used for various metals [42 – 44].

In our calculation, the interaction energy between Al_{22} and $C_{250}H_{52}$ nanoflake was determined by the Morse formula

$$E_{\text{Morse}} = \sum_i \sum_j D\left(\left(1-e^{-a(r_{ij}-R_0)}\right)^2 - 1\right). \qquad (4)$$

In this formula, the variables *i* and *j* number the aluminum and carbon atoms, respectively; r_{ij} is the corresponding Al-C interatomic distance; D, a, R_0 are the fitting parameters. The specific energy discrepancy per aluminum atom ΔE was calculated as the difference between two energies: $\Delta E = (E_{\text{DFT}} - E_{\text{Morse}})/N$, where $N = 22$ is the number of aluminum atoms, E_{DFT} is calculated with formula (1). We adopted a cutoff radius R_{cut} to be equal to 4 Å.

To get a set of non-equilibrium configurations of our system, we performed *ab initio* NVT molecular dynamics with a time step of 1 fs and a total time of 2 ps. Ten instantaneous configurations appeared every 0.2 ps were saved. Four of them are shown in Figs. 2 a – d. For each of these configurations, we

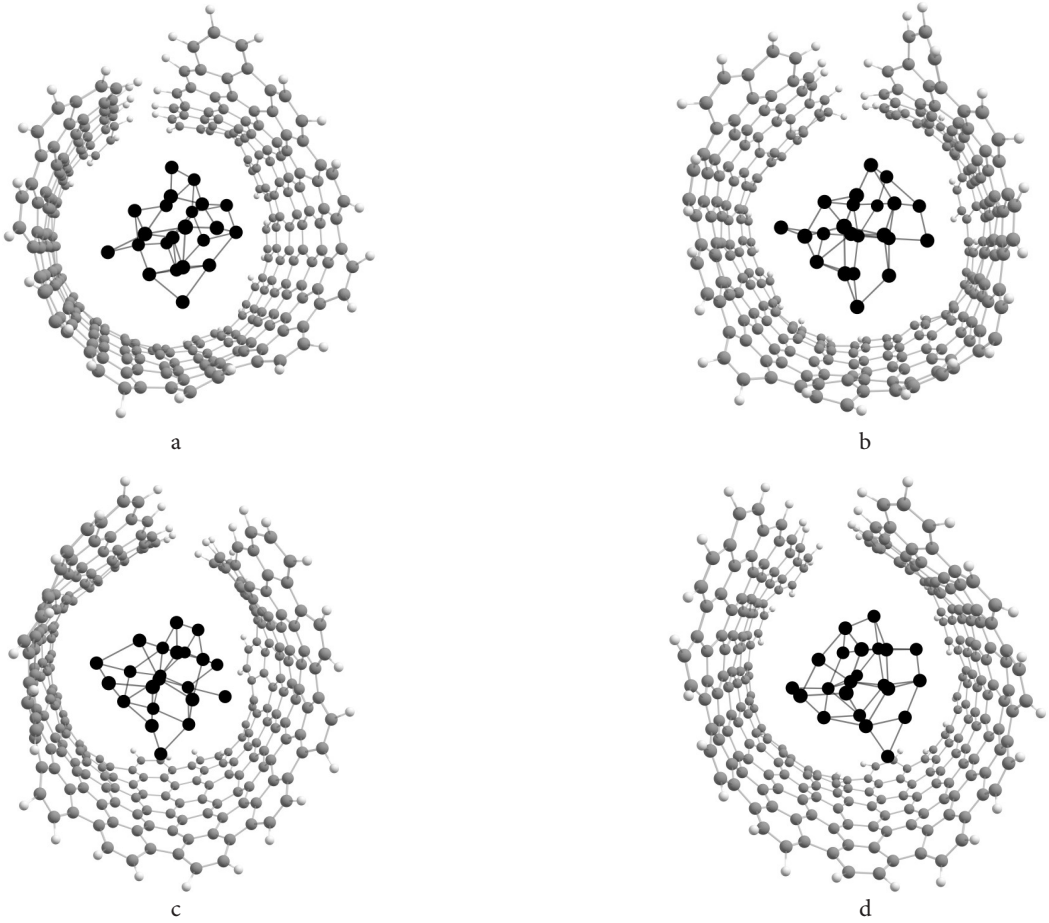

Fig. 2. Non-equilibrium configurations of the $Al_{22}@C_{250}H_{52}$ system after 0.5 ps (a), 1.0 ps (b), 1.5 ps (c) and 2.0 ps (d) molecular dynamics simulations.

calculated the interaction energies between the aluminum nanoparticle and nanoflake (E_{DFT} and E_{Morse}) as well as the energy discrepancies ΔE_k (k=1 to 10). The error measure, which quantitatively characterizes the adequacy of the Morse parameters, was calculated using the formula

$$error(D,a,R_0)=\sqrt{\frac{1}{10}\sum_{k=1}^{10}\left(\Delta E_k\right)^2}. \qquad (5)$$

Next, we fitted the parameters to minimize the *error* value, calculated with formula (5). The initial values of the parameters D, a and R_0 were randomly selected from the ranges 0 ÷ 5 eV, 0.1 ÷ 6 Å^{-1} and 2 ÷ 4 Å, respectively. We tried a thousand initial sets, which were then optimized by a simple gradient descent method. The best parameters found are presented in Table 1. From this table, one can see that the *error* value has decreased by more than ten times compared to the result obtained with the parameters from previous works [35,45]. As expected, the value of D was significantly lower for a concave surface, whereas the value of the equilibrium distance R_0 was considerably higher in comparison with the previously obtained data [35,45]. This discrepancy is due to the chemical inactivity of the concave carbon surface mentioned above.

Table 1. Morse parameters fitted for the Al-C interaction.

	D, eV	a, Å^{-1}	R_0, Å	R_{cut}, Å	*error*, eV
Qiu [35]	0.482	1.322	2.246	4.0	0.232
Fang-Wu [45]	0.809	1.860	2.970	4.0	0.330
This work	0.196	4.117	3.450	4.0	0.017

3.3. Al-C interaction in the Al@C_{60} metallofullerene

Next, we considered metallofullerene Al@C_{60}. The encapsulation energy Eenc of an aluminum atom inside a fullerene was 1.65 eV. High positive value of E_{inc} proves that the formation of metallofullerene is energetically feasible. The Mulliken charge of the aluminum atom is 0.73|e|, indicating a significant transfer of the positive charge from the fullerene to the aluminum. Table 2 presents the energies of the frontier orbitals of fullerene C_{60} and metallofullerene Al@C_{60}. One can see that the aluminum atom strongly distorts the energies of the frontier molecular orbitals and, consequently, changes the fullerene reactivity.

Note that the encapsulation energy E_{enc} is almost eight times higher than the parameter D presented in Table 1. Thus, the effect of aluminum on the carbon shell in the Al@C_{60} system is much more significant than a similar effect in the Al_{22}@$C_{250}H_{52}$ system.

Table 2. Energies of the frontier molecular orbitals HOMO and LUMO, HOMO-LUMO gaps and incorporation energy E_{enc} (see formula (2)) calculated for the Al@C_{60} metallofullerene.

	HOMO, eV	LUMO, eV	gap, eV	E^{enc}, eV
C_{60}	−5.50	−3.83	1.67	-
Al@C_{60}	−4.02	−3.96	0.06	1.66

3.4. Hydrogen bonding between fluorinated Al@C_{60} metallofullerene and niacin

Fluorinated carbon fullerenes are considered as promising drug carriers [46]. The strong electronegativity of fluorine ensures the formation of hydrogen bonds between the carrier and the drug. The additional charge of the metallofullerene carbon shell, appeared due to the electron density transfer from aluminum atom, can contribute to the formation of hydrogen bonds. Due to the strong interaction of fluorine atoms on the fullerene surface, they tend to be adsorbed in pairs, in para position relative to each other [46]. Thus, $C_{60}F_2$ is the smallest realistic model of fluorinated fullerene. Therefore, we considered the adsorption of niacin on $C_{60}F_2$ and Al@$C_{60}F_2$.

Frontier molecular orbitals, HOMO-LUMO gap and binding energies of corresponding compounds are listed in Table 3. Interestingly, that the presence of aluminum atom not only distorts the frontier orbitals, but also significantly reduces the binding energy between the fluorinated fullerene and the drug molecule. Thus, the carbon shell of metallofullerene becomes unsuitable for reliable loading of the niacin drug. We believe that a similar effect can be observed for other molecules that bind to the carrier by a similar mechanism through hydrogen bonds.

Table 3. Energies of the frontier molecular orbitals HOMO and LUMO, HOMO-LUMO gaps and binding energy E_b (see formula (3)) calculated for the niacin drug molecule adsorbed on fluorinated fullerenes $C_{60}F_2$ and Al@$C_{60}F_2$ metallofullerenes.

	HOMO, eV	LUMO, eV	gap, eV	E_b, eV
niacin	−6.05	−2.51	3.54	-
$C_{60}F_2$	−5.53	−4.12	1.41	-
Al@$C_{60}F_2$	−4.13	−4.06	0.07	-
$C_{60}F_2$ + niacin	−5.61	−4.23	1.37	0.52
Al@$C_{60}F_2$ + niacin	−4.22	−4.13	0.09	0.08

4. Conclusions

In the presented Letter, we have studied aluminum-carbon interaction in two core-shell complexes of different sizes, Al_{22}@$C_{250}H_{52}$ and Al@C_{60}. First of all, we determined the Morse parameters for the interaction of the aluminium nanoparticles with a concave carbon surface. We have demonstrated that the potential parameters are very different from the parameters for the more general case when the carbon surface is convex. Note that the classical molecular dynamics is an extremely powerful tool for the study of nanostructures. It provides an understanding of processes occurring on considerable time and spatial scales that are inaccessible to rigorous *ab initio* approaches. However, the predictive power of molecular dynamics is determined by the accuracy of the interatomic potentials used. Carbon nanostructures significantly change their chemical activity during bending. This fact should be carefully considered for the realistic modelling of such systems and composites based on them.

Then we considered the influence of Al core on the activity of carbon shell. We found that the Al_{22} nanoparticle do not lead to charge transfer and any significant difference

in shell reactivity due to the weak Al-C interaction. In contrast, in metallofullerene Al@C_{60}, the metal atom distorts frontier orbitals and reactivity. In particular, fluorinated metallofullerenes Al@$C_{60}F_2$ can not form the reliable hydrogen bonds with the niacin and others similar drugs. Therefore, carbon-coated aluminum can not be considered as a suitable drug carrier. We believe that the presented results will be helpful in modelling aluminum-doped carbon systems and can provide realistic predictions useful for the drug delivery, hydrogen storage, and other applications.

Acknowledgements. The presented study was performed with the financial support of the Russian Science Foundation (Grant No. 20-73-00245). Konstantin P. Katin is grateful to DSEPY-RI for the provided computing resources and software, as well as comprehensive support of the presented study.

References

1. L. L. Safina, J. A. Baimova, K. A. Krylova, R. T. Murzaev, R. R. Mulyukov. Lett. Mater. 10 (3), 351 (2020). Crossref
2. L. L. Safina, J. A. Baimova. Micro Nano Lett. 15, 176 (2020). Crossref
3. M. Barani, M. Mukhtar, A. Rahdar, G. Sargazi, A. Thysiadou, G. Z. Kyzas. Molecules. 26, 186 (2021). Crossref
4. S. Javanbakht, M. Pooresmaeil, H. Namazi. Carbohydrate Polymers. 208, 294 (2019). Crossref
5. B. P. Tarasov, A. A. Arbuzov, S. A. Mozhzhuhin, A. A. Volodin, P. V. Fursikov, M. V. Lototskyy, V. A. Yartys. Int. J. Hydr. Ener. 44, 29212 (2019). Crossref
6. M. Kaur, K. Pal, J. Mater. Sci: Mater. Electron. 31, 10903 (2020). Crossref
7. A. Ashok, A. Kumar, J. Ponraj, S. A. Mansour. Carbon. 170, 452 (2020). Crossref
8. W. Chen, J. Shen, Y. Huang, X. Liu, D. Astruc. ACS Sustainable Chem. Eng. 8, 7513 (2020). Crossref
9. M. Nasrollahzadeh, Z. Issaabadi, M. M. Tohidi, S. Mohammad Sajadi. Chem. Rec. 18, 165 (2017). Crossref
10. L. R. Safina, J. A. Baimova, R. R. Mulyukov. Mech. Adv. Mater. Mod. Process. 5, 2 (2019). Crossref
11. S. Tao, M. Yang, H. Chen, G. Chen. ACS Sustainable Chem. Eng. 6, 8719 (2018). Crossref
12. G. Darabdhara, M. R. Das, S. P. Singh, A. K. Rengan, S. Szunerits, R. Boukherroub. Adv. Colloid Interf. Sci. 271, 101991 (2019). Crossref
13. İ. Muz, M. Kurban, J. Mol. Liquids. 335, 116181 (2021). Crossref
14. M. Kurban, İ. Muz, J. Mol. Liquids. 309, 113209 (2020). Crossref
15. A. Kumar, D. Kumar. Bull. Mater. Sci. 43, 205 (2020). Crossref
16. İ. Muz, M. Atiş. J. Alloys Compounds. 667, 275 (2016). Crossref
17. G. Liu, J. Zhou, W. Zhao, Z. Ao, T. An. Chinese Chem. Lett. 31, 1966 (2020). Crossref
18. A. S. Ghasemi, F. Mashhadban, F. Ravari. Adsorption. 24, 471 (2018). Crossref
19. N. A. Monteiro-Riviere, S. J. Oldenburg, A. O. Inman. J. Appl. Toxicol. 30, 276 (2010). Crossref
20. W. J. Watterson, S. Moslehi, C. Rowland, K. M. Zappitelli, J. H. Smith, D. Miller, J. E. Chouinard, S. L. Golledge, R. P. Taylor, M.-T. Perez, B. J. Alemán. Micromachines. 11, 546 (2020). Crossref
21. X.-P. Zhao, S.-S. Wang, M. R. Younis, X.-H. Xia, C. Wang. Adv. Mater. Interfaces. 5, 1800185 (2018). Crossref
22. A. S. Ghasemi, F. Ashrafi, S. A. Babanejad, A. Elyasi. J. Struct. Chem. 60, 13 (2019). Crossref
23. S. Bagheri Novir, M. R. Aram. Physica E. 129, 114668 (2021). Crossref
24. M. Vatanparast, Z. Shariatinia. Struct. Chem. 29, 1427 (2018). Crossref
25. Y. Gao, L. Hu, Y. Liu, X. Xu, C. Wu. BioMed Research Intern. 2019, 1 (2019). Crossref
26. T. Wang, Y. Zhen, X. Ma, B. Wei, N. Wang. ACS Appl. Mater. Interfaces. 7, 6391 (2015). Crossref
27. K. A. Krylova, J. A. Baimova, I. P. Lobzenko, A. I. Rudskoy. Phys. B: Cond. Matter. 583, 412020 (2020). Crossref
28. K. Krylova, J. Baimova, R. Mulyukov. Lett. Mater. 9 (1), 81 (2019). Crossref
29. J. A. Baimova, B. Liu, S. V. Dmitriev, K. Zhou. J. Phys. D: Appl. Phys. 48, 095302 (2015). Crossref
30. C. Lee, W. Yang, R. G. Parr. Phys. Rev. B. 37, 785 (1988). Crossref
31. A. D. Becke. J. Chem. Phys. 98, 5648 (1993). Crossref
32. M. Tanaka, M. Katouda, S. Nagase. J. Comput. Chem. 34, 2568 (2013). Crossref
33. S. Grimme, J. Antony, S. Ehrlich, H. Krieg. J. Chem. Phys. 132, 154104 (2010). Crossref
34. S. Seritan, C. Bannwarth, B. S. Fales, E. G. Hohenstein, S. I. L. Kokkila-Schumacher, N. Luehr, J. W. Snyder Jr., C. Song, A. V. Titov, I. S. Ufimtsev, T. J. Martínez. J. Chem. Phys. 152, 224110 (2020). Crossref
35. C. Qiu, Y. Su, J. Yang, X. Wang, B. Chen, Q. Ouyang, D. Zhang. Composites B: Engineering. 220, 108996 (2021). Crossref
36. V. S. Prudkovskiy, K. P. Katin, M. M. Maslov, P. Puech, R. Yakimova, G. Deligeorgis. Carbon. 109, 221 (2016). Crossref
37. L. R. Safina, J. A. Baimova, K. A. Krylova, R. T. Murzaev, S. A. Shcherbinin, R. R. Mulyukov. Phys. Stat. Sol. RRL. 15, 2100429 (2021). Crossref
38. A. Y. Galashev. Int. J. Comput. Methods. 18, 2150032 (2021). Crossref
39. L. R. Safina, K. A. Krylova, R. T. Murzaev, J. A. Baimova, R. R. Mulyukov. Materials. 14, 2098 (2021). Crossref
40. A. V. Verkhovtsev, Y. Erofeev, A. V. Solov'yov. Eur. Phys. J. D. 74, 205 (2020). Crossref
41. A. Lyalin, A. Hussien, A. V. Solov'yov, W. Greiner. Phys. Rev. B. 79, 165403 (2009). Crossref
42. A. Y. Galashev, K. P. Katin, M. M. Maslov. Phys. Lett. A. 383, 252 (2019). Crossref
43. G. M. Poletaev, I. V. Zorya, R. Y. Rakitin, M. A. Iliina. Mater. Phys. Mech. 42, 380 (2019). Crossref
44. S. V. Kolesnikov, A. V. Sidorenkov, A. M. Saletsky. JETP Lett. 111, 116 (2020). Crossref
45. T.-H. Fang, J.-H. Wu. Comput. Mater. Sci. 43, 785 (2008). Crossref
46. E. B. Kalika, K. P. Katin, A. I. Kochaev, S. Kaya, M. Elik, M. M. Maslov. J. Mol. Liquids. 353, 118773 (2022). Crossref